Measurements of the diameter of rising gas bubbles by means of the ultrasound transit time technique

Richter, T.; Keplinger, O.; Strumpf, E.; Wondrak, T.; Eckert, K.; Eckert, S.; Odenbach, S.;

Originally published:

January 2018

Magnetohydrodynamics 53(2017)2, 383-392

Perma-Link to Publication Repository of HZDR:

https://www.hzdr.de/publications/Publ-25010

MEASUREMENTS OF THE DIAMETER OF RISING GAS BUBBLES BY MEANS OF THE ULTRASOUND TRANSIT TIME TECHNIQUE

T. Richter[1], *O. Keplinger*[2], *E. Strumpf*[2], *T. Wondrak*[2], *K. Eckert*[2], *S. Eckert*[2], *S. Odenbach*[1]

[1] *Chair of Magnetofluiddynamics, Measuring and Automation Technology, Institute of Fluid Mechanics, Technische Universität Dresden, D-01069 Dresden, Germany*
[2] *MHD Department, Helmholtz-Zentrum Dresden–Rossendorf (HZDR), PO Box 510119, D-01314 Dresden, Germany*
e-Mail: Thomas.Richter6@tu-dresden.de

This study presents ultrasound transit time technique (UTTT) measurements of single Ar bubbles rising in GaInSn under an applied magnetic field. Two setups were used to analyze the bubble rise, which led to differently oriented zig-zag trajectories. UTTT is able to visualize the bubble trajectory and to measure the variations of the apparent bubble diameters associated with the zig-zag trajectory. Due to the straightening of the bubble trajectories with increasing magnetic field, an increase of the apparent bubble diameter was detected.

Introduction. Mapping of fluid flow and detection of bubbles are important for opaque two-phase flows, such as liquid metal–gas flows as well as for opaque reactors. Ultrasound (US) techniques allow quantitative measurements in these cases. In particular, the ultrasound transit time technique (UTTT) possesses advantages for studying bubble distributions, the motion and contour dynamics of bubbles. The bubble motion has been studied in detail for bubbles rising in water. A bubble rises on a rectilinear motion when $\mathrm{Re} < 280$ (Saffman, Hartunian and Sears [1, 2]). For $\mathrm{Re} > 280$, the motion turns into a zig-zag trajectory (Magnaudet and Eames [3]) and later on into a helical motion (Ellingson and Riso [4]). Zhang *et al.* [5] investigated the rise of single bubbles in GaInSn and observed that the zig-zag motion of the bubble changed to a more rectilinear rise with a decreasing rising velocity when a high vertical magnetic field was applied. Simulations of this bubble rise were performed by Schwarz and Fröhlich and Ni and coworkers [6, 7]. They showed also a more rectilinear rise and the decreasing rising velocity of the bubble under a vertical magnetic field. A recent study of the group of Ni [8] gave a comprehensive overview about single bubbles rising in GaInSn in a magnetic field applied horizontally. They showed also for this field configuration that the rising speed of the bubble decreased upon increasing the magnetic field ($N < 1$). Furthermore, they predict that the bubble shape is elongated in the horizontal plane perpendicular to the magnetic field. By contrast, the shape parallel to the magnetic field is squeezed due the vortices generated on both bubble sides and to the overpressure associated with them. The group of Thomas and coworkers also simulated the rise of bubbles in liquid steel in a horizontal magnetic field [9]. They analyzed two bubble sizes, 3 mm ($\mathrm{Eo} = 0.51$) and 7 mm ($\mathrm{Eo} = 2.8$), for a magnetic field up to $B = 0.5\,\mathrm{T}$. The larger bubble (7 mm) showed a higher aspect ratio (the ratio between the major and the minor axis) of up to 2.63 and large shape oscillations at $B = 0.2\,\mathrm{T}$. Both bubble sizes showed a stabilized rise at $B = 0.5\,\mathrm{T}$. Interestingly, Thomas and coworkers found a slight elongation in the direction of the applied magnetic field in contrast to [8]. Beside these two numerical studies on

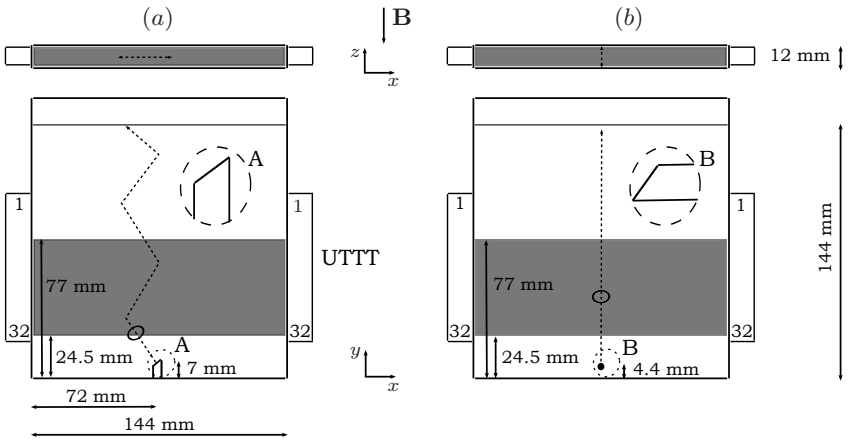

Fig. 1. Schematic diagram of the experimental setups from top and side view. The gray boxes indicate the measurement range. (*a*) The frst setup with the bubble injection through the vessel bottom. (*b*) The second setup with the bubble injection through the vessel wall. The position and shape of the orifice in both setups are shown as a zoom in the circular inset.

Table 1. Density, dynamic viscosity, surface tension, sound velocity and electrical conductivity of GaInSn at $\vartheta = 20°\mathrm{C}$ [10, 11].

ρ, [kg/m^3]	η, [mPas]	σ, [N/m]	c, [m/s]	σ_{el} [Ω^{-1}cm^{-1}]
6360	2.18	$533{\cdot}10^{-3}$	2730	32900

the rise of bubbles in a horizontal magnetic field and the resulting shape variation, experimental works are scarce. The present work aims to bring more insight into the behavior of the bubble diameter by investigating the rise of a single argon bubble in GaInSn.

1. Experimental setup. Fig. 1 shows the experimental setup that was used for the measurements of the bubble rise. An open vessel made of acrylic glass (wall thickness 2.0 mm) with an inner size of 144 mm × 12 mm was filled up to a height of 144 mm with GaInSn, the material data of which are collected in Table 1. A sharp injection needle, made of stainless steel, with an inner diameter of 0.785 mm was used as an orifice. The top of the needle was sharpened at an angle of 15° which caused the bubbles to detach in a preferred direction. As a result, the orientation of the plane for the bubble zig-zag motion could be adjusted. In the first setup, the needle was placed vertically in the center of the vessel, 7 mm above the bottom (Fig. 1*a*). In the second setup (Fig. 1*b*), the needle was inserted horizontally through the vessel wall, 4.6 mm above the bottom. This particular alignment of the needle ensured that the zig-zag motion took place in a plane parallel to the long wall of the vessel in the first setup and mainly perpendicular to the latter in the second configuration. Argon was injected into the liquid through these orifices with a sufficiently small flow rate of $Q_{\mathrm{g}} = 0.011\,\mathrm{cm}^3/\mathrm{s}$, which guaranteed a single bubble regime.

The UTTT transducer arrays, containing 32 elements of size 2.5 mm × 5 mm, were placed at the short side walls of the vessel. Table 2 gives the correlation between the couples of elements of the transducer array, referred as levels and their height in the vessel. According to Table 2, the measuring section starts at a height of 24.5 mm and ends 77.0 mm above the vessel ground. The ultrasound cones of

Table 2. Correlation between the transducer element couples used, referred to as *levels* in Fig. 4 and 8 and their height in the vessel.

Level	1	2	3	4	5
height above bottom, [mm]	24.5	37	49.5	62	74.5

the transducer array have an average thickness of 6 mm. With an average bubble velocity of 220 mm/s, the bubble has a residence time of about 30 ms in the US cone. For comparison, the transit of the US wave packets from the transducer to the bubble and back amounts 40 to 65 μs.

The measuring principle of UTTT is based on single US impulses emitted with a pulse repetition frequency f_p by a transducer and is described in detail in Andruszkiewicz *et al.* [12]. The transit times give access to the position of the bubble x_B and its apparent diameter d_B^ap. The position of the bubble follows from

$$x_\mathrm{B} = c \cdot t_\mathrm{B}/2, \tag{1}$$

where $t_\mathrm{B}/2$ is the time which the ultrasound needs to pass from the transducer to the bubble, and c is the sound velocity (Table 1). The apparent bubble diameter can be calculated by combining the signals in opposite transducer arrays (the subscripts i and j) according to

$$d_\mathrm{B}^\mathrm{ap} = D - x_{\mathrm{B}i} - x_{\mathrm{B}j}, \tag{2}$$

where D is the length of the long side of the vessel. The uncertainty of the d_B^ap determination by UTTT amounts to 7%. For more details we refer to Richter *et al.* [13].

To classify the bubble size, we introduce an equivalent bubble diameter, d_e, which assumes a spherical shape of the bubbles:

$$d_\mathrm{e} = \left(\frac{V}{n} \cdot \frac{6}{\pi} \right)^{1/3}, \tag{3}$$

V is the gas volume and n the number of bubbles in this volume. A typical value for our argon bubble in GaInSn is $d_\mathrm{e} = 5$ mm. This clearly points to bubbles of an ellipsoidal shape, as was also verified by X-ray radiography, Richter *et al.* [14]. Hence, it is more convenient to characterize the bubbles by means of the large and short axes, d_1 and d_2, of the equivalent ellipsoid. The aspect ratio a_r of the ellipsoid is given by

$$a_\mathrm{r} = \frac{d_2}{d_1} \tag{4}$$

and was determined from X-ray radiography [14]. Then the diameter of the shorter axis follows from

$$d_1 = \left(\frac{V}{n} \cdot \frac{6}{\pi a_\mathrm{r}^2} \right)^{1/3}. \tag{5}$$

The horizontal magnetic field was generated by means of a DC electromagnet, the magnetic induction B of which ranged from 0 to 505 mT. The vessel was positioned such that the magnetic field was directed perpendicular to the long side of the vessel. For a classification of the bubble dynamics and magnetic field, we introduce the Hartmann number $\mathrm{Ha} = B \cdot d_\mathrm{e} \sqrt{\sigma_\mathrm{el}/\eta}$, the Stuart number, or the magnetic interaction parameter $\mathrm{N} = \sigma_\mathrm{el} B^2 d_\mathrm{e}/(\rho u)$ (u is the terminal rising velocity of the bubble) and the Eötvös number $\mathrm{Eo} = (\rho_\mathrm{l} - \rho_\mathrm{g}) \cdot g d_\mathrm{e}^2/\sigma$.

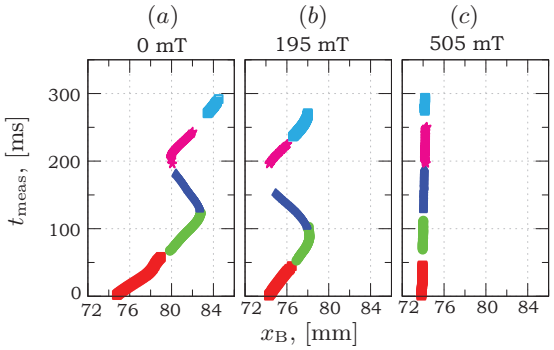

Fig. 2. First setup: bubble trajectories (bubble position x_{B}) without a magnetic field (a), $N = 0.5$ (b), $N = 3.4$ (c).

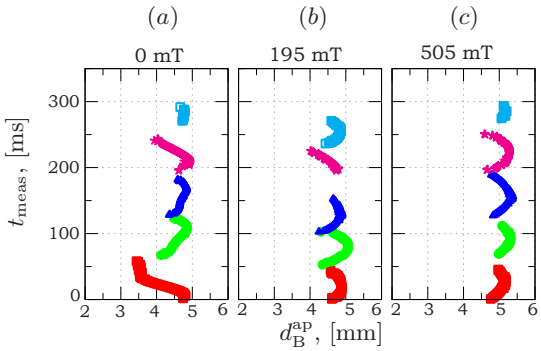

Fig. 3. First setup: apparent bubble diameters $d_{\mathrm{B}}^{\mathrm{ap}}$ without a magnetic field (a), $N = 0.5$ (b), $N = 3.4$ (c).

2. Results and discussion.

2.1. First setup. In this setup, argon is injected from the vessel bottom and a planar zig-zag motion parallel to the long vessel walls is adjusted, i.e. in a plane perpendicular to the applied magnetic field. The rising bubbles with no applied magnetic field had an averaged volume of 74.62 mm^3, corresponding to $d_{\mathrm{e}} = 5.22$ mm, or $d_1 = 4.38$ mm and $d_2 = 5.7$ mm, taking the aspect ratio $a_{\mathrm{r}} = 1.3$, averaged over the bubble rise, measured by X-ray radiography at $B = 0$. The Eötvös number for d_{e} was Eo $= 2.9$. The volume emerging from the nozzle increased up to 83.29 mm^3 at $B = 505$ mT, which led to a $d_{\mathrm{e}} = 5.42$ mm (Eo $= 3.13$), or $d_1 = 4.55$ mm and $d_2 = 5.91$ mm. Here, the same $a_{\mathrm{r}} = 1.3$ was assumed as measured in the case of N $= 0$. Fig. 2 shows three bubble trajectories: one without the applied magnetic field, one at $B = 195$ mT (N $= 0.5$, Ha $= 42$) and the third at $B = 505$ mT (N $= 3.4$, Ha $= 109$), plotted over the measuring time t_{meas}. Without the applied magnetic field, the planar zig-zag trajectory was inclined. This is visible in the displacement of the reversal points in Fig. 2a. Note the different horizontal position of the first reversal point and of the third one, which is located immediately at the end of the blue curve segment, cf. also Fig. 2b. When the magnetic field was increased, the zig-zag trajectory was straightened and approached a rectilinear rise at N $= 3.4$ (Fig. 2c). Alongside, the inclination of the trajectory is suppressed, we see nearly identical horizontal positions of the first and third reversal points in Fig. 2b. Fig. 3 plots the apparent bubble diameters measured along the bubble trajectories of the same bubbles shown in Fig. 2. If no magnetic field is applied (N $= 0$), the apparent diameter of the bubbles undergoes significant variations during the rise of the bubble (Fig. 3 a). It is known that during the

zig-zag rise the bubble tilts its short axis such that it is parallel to the velocity vector. Depending on the tilt at the specific level, different maximum apparent diameters are measured by UTTT. Hence, the differences of the apparent diameters between different levels are related to the dynamics of the bubbles. With increasing N, the d_B^{ap} curves of the different levels become more and more similar and approach a parabolic shape (Fig. 3*c*). Furthermore, the maximum apparent diameter shows the tendency to increase with increasing applied magnetic field from around d_B^{ap} 4.8 mm to 5.4 mm at N = 3.4 (Fig. 3*c*). To a large extent, this is caused by a reduction of the tilt of the bubbles. In case of a straight bubble trajectory, the tilt vanishes. Hence, the bubble rises with its large axis in the horizontal position. It is clear that the apparent diameter measured by UTTT, corresponding in this case to d_2, is larger than that of a bubble undergoing a zig-zag motion. To a smaller extent, the increase of d_B^{ap} with B results from an increasing bubble volume as discussed later on. The stretching of the bubble, as predicted by Ni *et al.* [8], could not be observed. This indicates that the stretching is smaller than the measuring error of UTTT.

Fig. 4 shows the maximum apparent bubble diameters measured at the five height levels versus the magnetic field applied. The bubble diameters were obtained after averaging over all bubbles at the respective height level. The error bar specifies the standard deviation. The rather high value of the latter at small magnetic fields results from the fact that, although the single bubbles move over similar trajectories, small fluctuations in amplitude of the zig-zag motion or in height of the reversal points occur. These fluctuations are responsible for a scatter of the measured values of the apparent diameters. Note that this scatter decreases with increasing applied magnetic field which is related to the more rectilinear rise of the bubbles.

To understand why the apparent bubble diameters curves in Fig. 3 display parabolic arcs, the bubble rise is simulated by means of a ray tracing algorithm. Ray tracing has already been successfully applied to evaluate and understand ultrasound tomography approaches (Andersen and Langener *et al.* [15, 16]). Ray tracing considers the local normal vector of the wavefronts of the ultrasound wave package emitted from the known transducer surface as a ray. If the ray hits the bubble surface, it is reflected. Some of these rays again reach the transducer

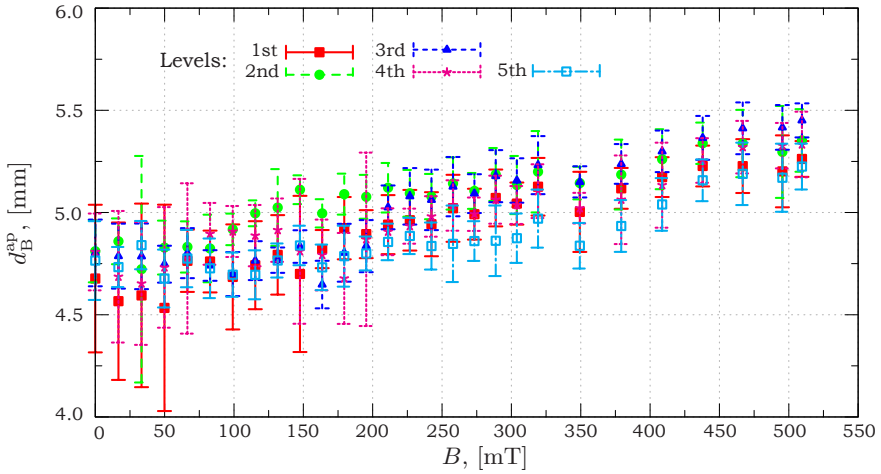

Fig. 4. First setup: maximum apparent diameter d_B^{ap} for specific levels, i.e. heights, plotted over the applied magnetic field.

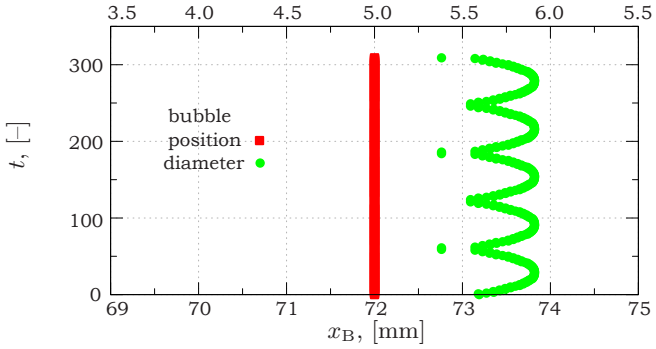

Fig. 5. Ray tracing simulation of an ellipsoidal bubble rising over a straight path. The red curve visualizes the bubble position and the green curve the apparent bubble diameter.

surface. The time between emission and detection is measured from which the object position and the apparent diameter can be calculated by analogy with UTTT. The bubble object was simulated as an ellipsoid of roation, oriented with the minor axis into the direction of the rise. The bubble size was calculated by the equivalent bubble volume measured during the UTTT measurements and by the aspect ratio measured via X-ray radiography. The transducer surfaces in the simulation had the same size and distances to each other as the transducer elements of the arrays used in the measurements.

To explain the behavior in Fig. 3, it is sufficient to simulate a straight trajectory of the bubble taking place at the same distance from the transducer as in the experiment. This straight path corresponds well to the bubble trajectory observed at N = 3.4. The results of the simulation are shown in Fig. 5. Note that the simulated shape of the apparent diameter curves reproduces the experimentally observed one (Fig. 3*c*) quite well. The detected parabolic shape was also observed earlier in experiments with falling steel balls (Richter *et al.* [13]) and is explained by the entry and exit effects of the round object in the ultrasound beam. The apparent diameter, i.e. the length of the ellipsoid of rotation in a horizontal cut, is small, when the tip of the ellipsoid just enters the US beam. It increases during the travel of the ellipsoid through the beam until the ellipsoid crosses the center of the ultrasound cone with its maximum lateral extension. Here, the maximum value of the apparent diameter was measured. When the ellipsoid starts to move out of the ultrasound cone, the apparent diameter decreases again in a symmetric way compared to the entry. Although the parabolic shapes of the diameter curves agree favorably well with the experiments, the simulations tend to overestimate the maximum bubble diameter by 9 to 10%, which, however, correlates with the uncertainty of the measurement method.

2.2. Second setup. Next, the sharp injection needle is placed horizontally in the vessel wall, cf. Fig. 1*b*. By this means, a zig-zag motion was forced perpendicular to the long vessel walls and parallel to the applied magnetic field. Without applying a magnetic field, the bubbles had an averaged volume of 87.98 mm^3. This corresponds to $d_e = 5.52$ mm (Eo = 3.25), or $d_1 = 4.63$ mm and $d_2 = 6.02$ mm at the given $a_r = 1.3$. In the presence of $B = 505$ mT, the volume emerging from the nozzle increased up to 98.27 mm^3. This leads to $d_e = 5.73$ mm (Eo = 3.5), or $d_1 = 4.81$ mm and $d_2 = 6.25$ mm at $a_r = 1.3$.

Based on the experiences with the first setup and reference experiments in water, it could be assumed that the present needle and orifice orientation gives rise to a zig-zag motion parallel to the short sides of the vessel (the z-direction in

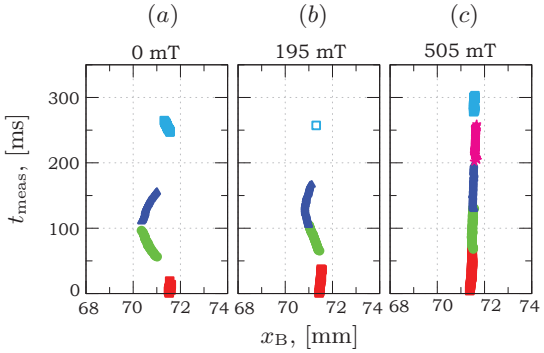

Fig. 6. Second setup: bubble trajectories (bubble position x_{B}) without a magnetic field (a), N = 0.5 (b), N = 3.6 (c).

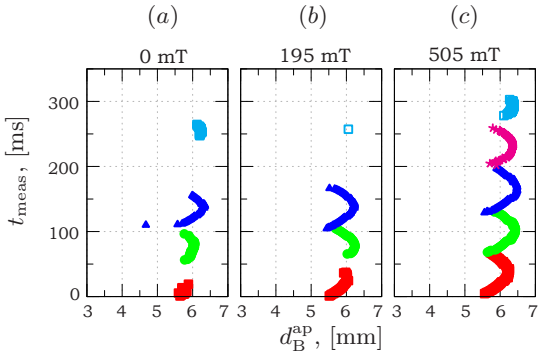

Fig. 7. Second setup: apparent bubble diameters $d_{\mathrm{B}}^{\mathrm{ap}}$ without a magnetic field (a), N = 0.5 (b), N = 3.6 (c).

Fig. 1). Hence, no bubble motion should occur in the direction of the transducer arrays (the x-direction in Fig. 1). Thus the expectation was to measure constant transit times which the ultrasound need for propagating between the transducer and the bubble and back. However, this expectation is not supported by the measurements plotted in Fig. 6 which shows three trajectories, one without the applied magnetic field, one at $B = 195\,\mathrm{mT}$ (N = 0.5, Ha = 44) and one at $B = 505\,\mathrm{mT}$ (N = 3.6, Ha = 115).

It is obvious that besides the motion along the z-direction also a motion along the x-direction occurred at zero and moderate magnetic fields (Fig. 6a,b). This observation is only compliant with the fact that the bubbles soon performed a helical motion which is straightened again with the increased magnetic field. Furthermore, no signal was detected for level 4, which means that the bubble path lies outside the US beam. With increasing magnetic field, hence, more rectilinear trajectories occurred, the signals of level 4 recovered again. Fig. 7 displays the apparent bubble diameters for the bubbles shown in Fig. 6. The trend towards a parabolic shape with the increasing magnetic field for all levels is similar to the trend found already in the first setup (Fig. 7c).

Fig. 8 shows the maximum apparent bubble diameters averaged over all bubbles versus the magnetic field applied. The deviation again results from the small fluctuations in the trajectories for the different bubbles and decreases again for the increasing magnetic field. The maximum apparent diameters grows only slightly from around $d_{\mathrm{B}}^{\mathrm{ap}}$ 6.1 mm up to 6.35 mm which, however, remains within the uncertainty of UTTT. The difference between the apparent diameter values

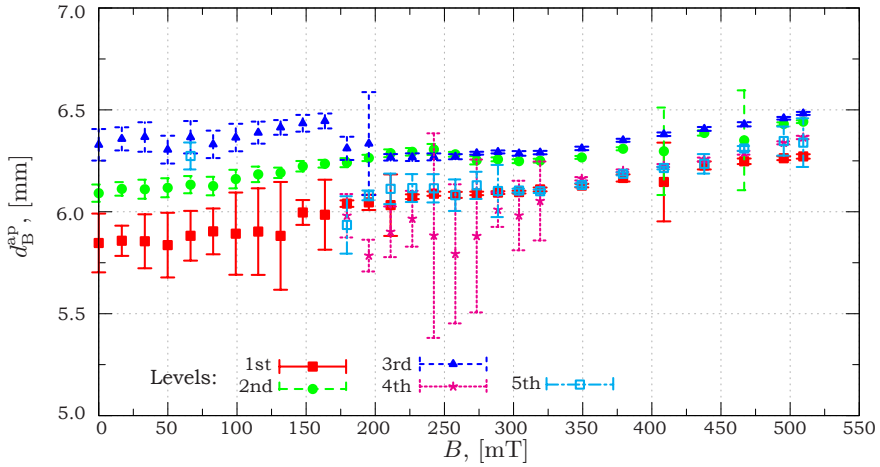

Fig. 8. Second setup: maximum apparent diameters d_B^{ap} with deviation for specific levels plotted over the applied magnetic field.

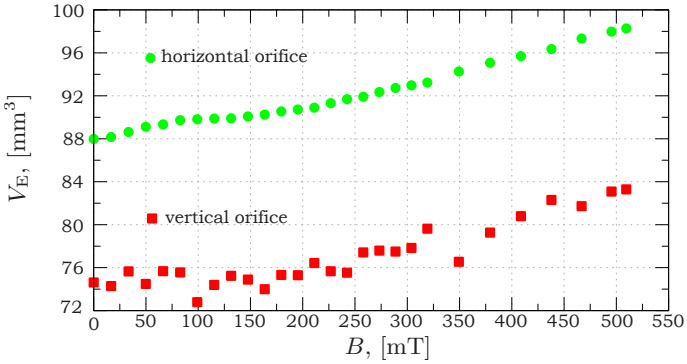

Fig. 9. Averaged bubble volumes plotted over the applied magnetic field for both orifice orientations: vertical orifice (first setup) and horizontal orifice (second setup).

and the different levels decreased again with the magnetic field caused by the more rectilinear bubble trajectory.

In Fig. 9 we plot the volume of the bubbles injected into the two setups. It is obvious that the bubble has a larger volume in the second setup compared to that in the first setup. This is attributed to the different orientation of the needle. The tip of the needle with its sharp edge, cf. Fig. 1, from which the bubble detaches, has a different projected area, depending on whether the needle is oriented horizontally or vertically. When the needle is positioned horizontally, the projected surface is larger and the bubble needs a 1.2 times larger volume to detach if compared to the first setup. In both setups, the averaged bubble volume increases with the magnetic field applied. Fig. 9 shows an expansion by approximately 12% between $B = 0$ and $B = 505\,\mathrm{mT}$. This increase of the bubble volume could be explained by the Lorentz force. The bubble pushes the GaInSn aside when it grows. For increasing B, the Lorentz force counteracts this displacment of the fluid and the bubble has to aquire a larger volume to produce enough lift in order to detach.

This increase of the bubble volumes with the magnetic field is the second source for the larger apparent diameters measured at higher N as discussed before. This behavior of the bubble volume complicates it further to extract the predicted stretching of the bubble from the UTTT data.

Conclusions. The rise of a single argon bubble in GaInSn was investigated by means of UTTT for two different orifice configurations in the presence of a horizontal magnetic field. The bubble performs a zig-zag, namely, a helical rise which was straightened to a nearly linear rise at $B = 505\,\mathrm{mT}$. In parallel, the tilt of the bubbles is clearly diminished.

The apparent bubble diameters are different for the two orifice configurations. This is caused by the larger bubble volume which is injected in the second setup. Furthermore, the volume of the bubbles increases with the magnetic field, which was explained by the damping effect of the Lorentz force. Further efforts are needed to verify whether an elongation of the bubble in the presence of the magnetic field occurs as predicted by numerical simulations.

Acknowledgments. Financial support by the Helmholtz Alliance LIMTECH (pro-ject YIG) and by German Federal Ministry for Economic Affairs and Energy under contract No. GRS-1501449 is gratefully acknowledged.

References

[1] P. Saffman. On the rise of small air bubbles in water. *Journal of Fluid Mechanics*, vol. 1 (1956), no. 03, pp. 249–275.

[2] R.A. Hartunian and W. Sears. On the instability of small gas bubbles moving uniformly in various liquids. *Journal of Fluid Mechanics*, vol. 3 (1957), no. 01, pp. 27–47.

[3] J. Magnaudet and I. Eames. The motion of high-reynolds-number bubbles in inhomogeneous flows. *Annual Review of Fluid Mechanics*, vol. 32 (2000), no. 1, pp. 659–708.

[4] K. Ellingsen and F. Risso. On the rise of an ellipsoidal bubble in water: oscillatory paths and liquid-induced velocity. *Journal of Fluid Mechanics*, vol. 440 (2001), pp. 235–268.

[5] C. Zhang, S. Eckert, and G. Gerbeth. Experimental study of single bubble motion in a liquid metal column exposed to a dc magnetic field. *International Journal of Multiphase Flow*, vol. 31 (2005), no. 7, pp. 824–842.

[6] S. Schwarz and J. Fröhlich. Numerical study of single bubble motion in liquid metal exposed to a longitudinal magnetic field. *International Journal of Multiphase Flow*, vol. 62 (2014), pp. 134–151.

[7] J. Zhang and M.-J. Ni. Direct simulation of single bubble motion under vertical magnetic field: Paths and wakes. *Physics of Fluids (1994-present)*, vol. 26 (2014), no. 10, p. 102102.

[8] J. Zhang, M.-J. Ni, and R. Moreau. Rising motion of a single bubble through a liquid metal in the presence of a horizontal magnetic field. *Physics of Fluids (1994-present)*, vol. 28 (2016), no. 3, p. 032101.

[9] K. Jin, P. Kumar, S. Vanka, and B. Thomas. Rise of an argon bubble in liquid steel in the presence of a transverse magnetic field. *Physics of Fluids (1994-present)*, vol. 28 (2016), no. 9, p. 093301.

[10] N. Morley, J. Burris, L. Cadwallader, and M. Nornberg. Gainsn usage in the research laboratory. *Review of Scientific Instruments*, vol. 79 (2008), no. 5, p. 056107.

[11] Y. Plevachuk, *et al.* Thermophysical properties of the liquid ga–in–sn eutectic alloy. *Journal of Chemical & Engineering Data*, vol. 59 (2014), no. 3, pp. 757–763.

[12] A. Andruszkiewicz, K. Eckert, S. Eckert, and S. Odenbach. Gas bubble detection in liquid metals by means of the ultrasound transit-time-technique. *The European Physical Journal Special Topics*, vol. 220 (2013), no. 1, pp. 53–62.

[13] T. Richter, K. Eckert, X. Yang, and S. Odenbach. Measuring the diameter of rising gas bubbles by means of the ultrasound transit time technique. *Nuclear Engineering and Design*, vol. 291 (2015), pp. 64–70.

[14] T. Richter, *et al.* Single bubble rise in GaInSn in presence of a horizontal magnetic field. *In progress*.

[15] A.H. Andersen. A ray tracing approach to restoration and resolution enhancement in experimental ultrasound tomography. *Ultrasonic Imaging*, vol. 12 (1990), no. 4, pp. 268–291.

[16] S. Langener, M. Vogt, H. Ermert, and T. Musch. Evaluation of results from ultrasound process tomography of multiphase media. *7th International Symposium on Process Tomography*, (2015).